Robert Hahn*, Yujia Yang, Uwe Maaß, Leopold Georgi, Jörg Bauer and K.-D. Lang

Variable Capacitor Energy Harvesting Based on Polymer Dielectric and Composite Electrode

DOI 10.1515/ehs-2016-0008

Abstract: This work focuses on a polymer based capacitive harvester which can be fabricated with help of roll-to-roll and low cost printing methods. In contrast to electrostatic MEMS based parallel plate transducers or dielectric elastomer systems here, the capacitance is varied as function of the mechanical load by changing of the top electrode area with help of an electrically conducting composite elastomer. In case of a composite elastomer electrode the maximum capacitance in compressed state does not only depend on the thickness and permitivity of the dielectric but first of all on the quality of the interface and the micro structure of the conducting phase in the composite electrode at the interface which was investigated by FEM Maxwell simulation. An equivalent circuit model is used to study the influence of the leakage current inside the dielectric and the bulk resistivity of the elastomer electrode. First experiments with state of the art polymer, thin film and novel printed dielectrics in contact with elastomer electrodes have been performed to prove the harvesting principle at low frequencies. Charges between 25 and 70 nAs per cm^2 have been transferred per cycle at 100 V/200 V while the maximum capacity was between 0.4 and 0.8 nF/cm^2.

Keywords: energy harvesting, capacitive transducer, composite polymer, high-k dielectric, equivalent circuit

Introduction

Energy harvesters with significantly improved power density and efficiency will be a crucial technology for many applications, including wearable and portable electronics, wireless sensor networks, the Internet of Things scheme, medical implants and others. In addition, fully energy autonomous micro systems will lead to completely new and innovative products in the future.

For the power supply of self- or low powered applications so far only photovoltaic energy harvesters are in wide spread use due to their sufficient power density and the availability of light. Thermoelectric converters can have a high power density, but need high temperature gradients which preclude their integration into commodity user items. Mechanical energy can be converted into electricity by piezoelectric, electromagnetic and electrostatic principle, but so far all these mechanical harvesters serve only niche applications, due to their low conversion efficiency, low power density and high cost.

The substantial amount of energy produced by the human body motivates the development of harvesters that could extract a part of it. Photovoltaic and thermal energy are not applicable or lead to awkward designs since the body or clothing are mostly opaque and thermo-regulated, while the body provides a continuous source of mechanical or vibrational energy for example from inertia, muscle contraction, heart beats, joint movement or heel strike. Additionally, the mechanical harvesters can be properly encapsulated in a package which increases long term stability and helps biocompatibility and integration. Scavenging low-frequency energy from regular and irregular bio-motion will be the main motivation for this work. It is anticipated to be feasible and practical to embed these devices into clothes, built in surface layers, and place them onto in-shoe pads for harvesting low-frequency energy in the range between 0.1 and 10 Hz. Other applications may include smart bandages and later implanted devices which extract energy from muscle movement. As the elastomers developed for the capacitive harvester mature, higher frequency up to 100 Hz may be investigated to widen the application spectrum to other ambient vibrating sources.

The energy conversion mechanism of an electrostatic transducer is based on the physical coupling of the electrical and the mechanical domain by an electrostatic

***Corresponding author: Robert Hahn,** Fraunhofer IZM, Gustav-Meyer-Allee 25, 13355 Berlin, Germany, E-mail: robert.hahn@izm.fraunhofer.de
Yujia Yang, Uwe Maaß, Fraunhofer IZM, Gustav-Meyer-Allee 25, 13355 Berlin, Germany
Leopold Georgi, Technische Universität Berlin, TiB4/2-1, Gustav-Meyer-Allee 25, 13355 Berlin, Germany
Jörg Bauer, Fraunhofer IZM, Gustav-Meyer-Allee 25, 13355 Berlin, Germany
K.-D. Lang, Technische Universität Berlin, TiB4/2-1, Gustav-Meyer-Allee 25, 13355 Berlin, Germany

force. The electrostatic force is induced between opposite charges stored on two opposing electrodes. The energy E stored in the electric field between the electrodes depends only on the capacity C and voltage V according to the equation

$$E = 1/2 \cdot C \cdot V^2 \quad [1]$$

In order to convert mechanical energy into electrical energy by means of the electrostatic transduction mechanism, a variation of capacitance over time must occur. For this purpose, state of the art harvesters use variable area-overlap or variable gap-closing parallel plate capacitors (Sheu et al. 2011; Lu, Cottone, and Boisseau 2016) with moving plates or alternatively dielectric elastomers (Lv et al. 2015; Zhang et al. 2015).

Here a new principle will be shown were the area of a deformable electrode is varied and changes the effective electrode area on a high-k dielectric (Figure 1). One type of such capacity variation was first described as "R-EWOD" (Reverse-Electrowetting-On-Dielectric) whereby an electrically conducting liquid metal (Mercury, Galinstan ®) droplet is deformed by the applied force (Krupenkin and Taylor 2011; Hsu et al. 2015). This concept was further thermodynamically elaborated and extended to any type of liquid bridges between oscillating electrodes (Janssen, Werkhoven, and van Roij 2016). We also tested this concept and confirmed that Galinstan is well suited for the use as reversibly deformable electrode due to its high electrical conductivity and high surface tension. On the other hand a simple technical realization is restricted by its high oxidation tendency. Galinstan electrodes work only under complete absence of oxygen or in lactic acid which imply a very high technical effort in terms of hermetic packaging that contradict with the low cost approach of this work. Therefore we decided to use electrically conducting elastomers as deformable electrodes to improve the prospects for efficient large-area fabrication.

The use of elastomer electrodes provides an advantage for portable, wearable and medical electronics applications, due to the inherent mechanical impedance match of the used polymers to human movement. This characteristic improves upon the known art in conventional electromagnetic and piezo harvesters which often require expensive and sophisticated gear transmission mechanisms. The harvester can be optimized for the frequency range between 0.1 and 10 Hz compatible to biomechanical and portable electronics applications.

During each cycle, an electronic circuit extracts energy, and feeds it into the energy storage device. The energy harvested by the variable capacitor per actuation cycle is proportional to the area change of the variable electrode and the maximum capacity per area.

While thin printable elastomer electrodes and dielectric layers offer obvious fabrication, cost and integration advantages, several issues have to be considered:

- The capacity per area will be smaller compared to a (liquid) metal electrode.
- Low efficiency due to elastic/viscoelastic deformation and material fatigue.
- Adhesive forces between dielectric and elastomer may result in delayed electrode release and will allow only low frequency operation.

In order to better understand the impact of the composite morphology of the elastomer electrode on the specific capacity and the requirements for material properties of elastomer electrode and dielectric we started with numerical simulations which are shown in Section "Simulation" while the experimental results are provided in Section "Experimental".

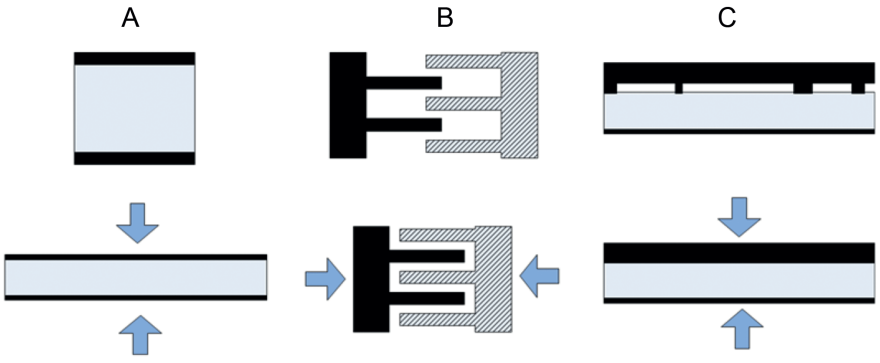

Figure 1: Variable capacitor principal configurations (A) dielectric elastomer, (B) parallel plate, (C) elastomer electrode, top: low capacity, bottom: high capacity.

Simulation

FEM Maxwell Simulation of a Capacitor with Composite Electrode

The investigated mechanically flexible elastomer electrode is a composite material which consists of a base polymer and electrically conducting fillers like carbon black, carbon nano-tubes or silver flakes. Hence there will be randomly distributed contacts between the electrically conducting phase and the dielectric and not a homogeneous interface. For the conducting filler particles which not contact the dielectric interface, the electrical field will penetrate through both, the low-k dielectric of the elastomer electrode and the high-k dielectric on the substrate. In addition air may be entrapped at the interface which further reduces the active capacitor area as demonstrated in Figure 2(A). To study the influence of the contact morphology on the specific capacity a 2D electrostatic FEM simulation (AnsysEM Maxwell) was performed were the filler particles are represented by electrically conducting fins as shown in Figure 2(A). An offset y was assumed that represent the case that the filler particles do not contact the interface and are covered with the matrix polymer of the composite electrode. In a first stage the model convergence was tested. At least 12 passes were required to achieve $\Delta C < 1\%$ for all parameter variants. The results shown in Figure 2(C) indicate that thin layers of dielectric over the conductor phase (fin offset) degrade the capacity greatly; even if there is no fin offset a large distance between the fibers (10 µm) reduces the resulting capacity significantly. Even a very large permittivity of the dielectric can't compensate the shortcomings of the elastomer electrode. This result is plausible as the set-up can be understood as a serial connection of a high and a low capacitor. In conclusion, the conductive phase should be distributed on the surface of the elastomer as homogeneous as possible with a mean distance below ca. 1 µm.

Calculation of Losses with the Equivalent Circuit Model

The conductivity of the elastomer electrode may be several orders of magnitude lower than that of metal electrodes. The high-k dielectric have to be deposited with a low cost printing process that may be prone to pin holes and

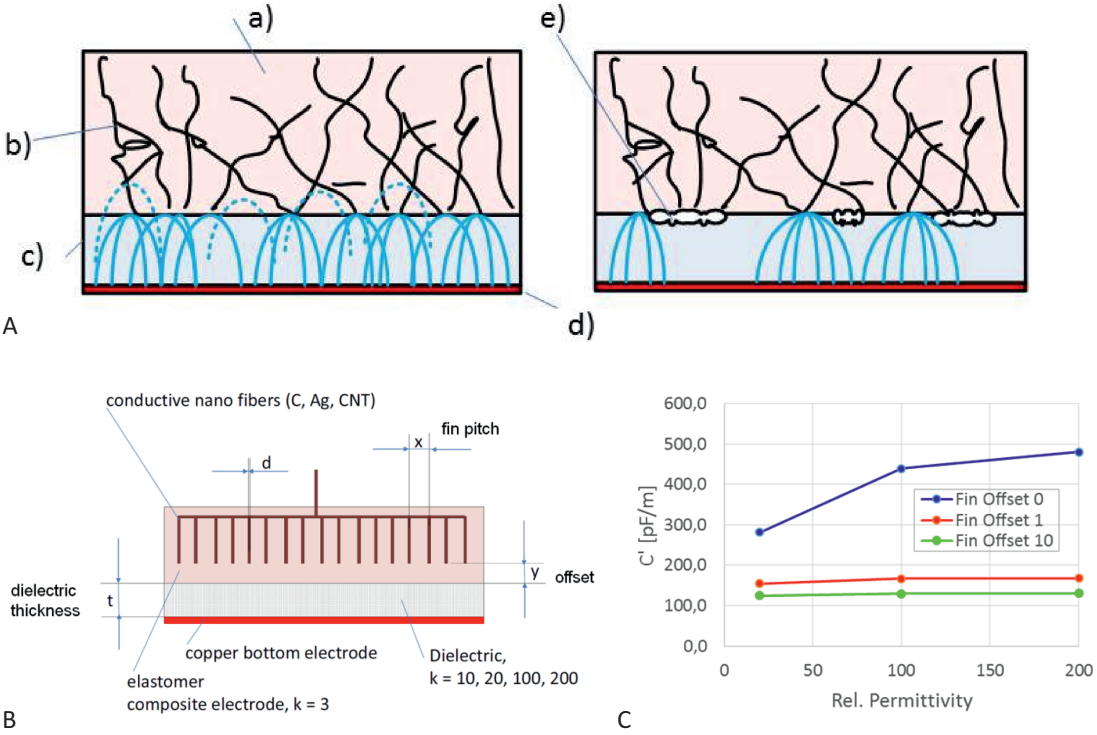

Figure 2: (A) Illustration of electrical field distribution, a) elastomer matrix polymer, b) interconnected conducting phase, c) high-k dielectric, d) bottom electrode, e) air entrapment, (B) FEM model, (C) simulated specific capacity as function of fin offset and relative permittivity of the dielectric (dielectric thickness t = 20 µm, fin width d = 0.1 µm, fin pitch x = 10 µm).

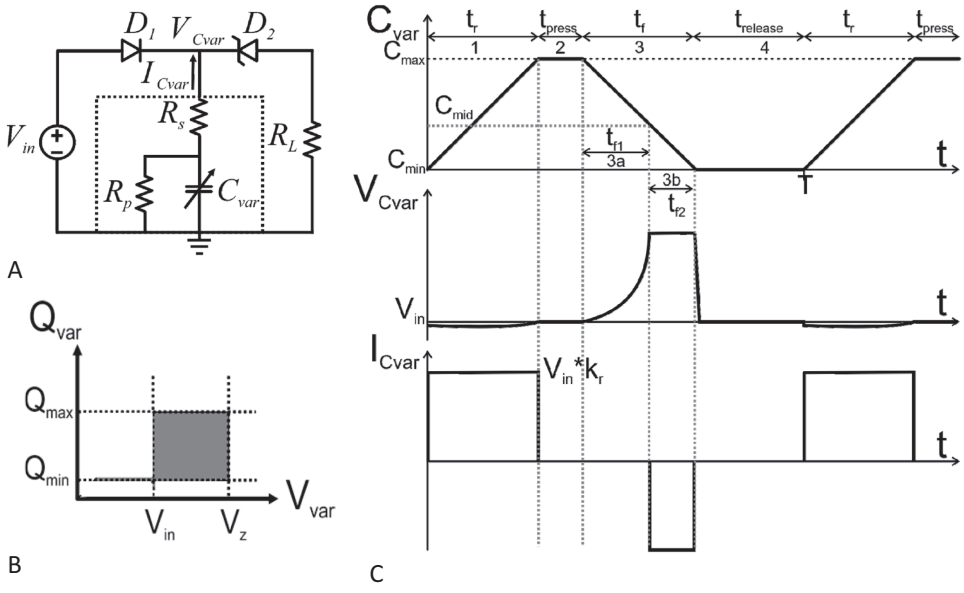

Figure 3: (A) The equivalent circuit of the investigated energy harvesting system, (B) The voltage and current waveforms of the harvester corresponding to the variation of capacitance, (C) Charge-voltage diagram showing the rectangular Q-V harvesting cycle.

resulting leakage currents. Therefore in order to analyze the efficiency of the capacitive harvester, an equivalent circuit was evaluated which includes parasitic resistances that represent leakage current and conduction losses as illustrated in Figure 3(A). The schematic represents the ideal conditioning circuit implementing a rectangular charge voltage cycle as shown in Figure 3(B) (Galayko and Dudka 2015). The *D2* Zener diode was used to establish a constant output voltage V_z. In a real harvesting situation *D2* would not be a Zener diode but same as *D1* which is conducting during phase 3 in order to charge the output capacitor which takes the place of R_L. We have used the circuit shown in Figure 3(A) to make clear that we evaluate the role of the parasitic elements under idealized conditions of fixed output voltage V_z. The assumed harvesting power is I_{CVAR}* V_Z during t_{f2}. C_{var} represents the ideal variable capacitor. R_s and R_p are the serial and parallel parasitic resistances of the harvester, which represent losses due to the resistivity of the elastomer electrode and the leakage current of the dielectric respectively. C_{var}, R_s and R_p all together in the dashed line compose the simplified model of the capacitive harvester. The analysis results of the losses will be used to guide the harvester design. In that way, the appropriate dielectric and electrode material will be selected or developed to fulfill the requirements for efficient energy harvesting.

Considering that the C_{var} can be stimulated with different form of forces, the capacitance of C_{var} will also vary accordingly in different waveforms. To simplify the analysis, a periodical capacitance variation as shown in Figure 3(C) has been used in this work to calculate the losses in R_s and R_p.

A complete energy harvesting cycle of the harvesting circuit can be divided into 4 intervals as depicted in Figure 3(C).

Interval 1: The harvester is pressed with a force and the capacitance is rising from $C_{\min}$ to $C_{\max}$. The voltage drop over the harvester V_{Cvar} is slightly smaller than the input voltage V_{in}. There is a current flowing from V_{in} to charge up the harvester capacitor until V_{Cvar} reaches V_{in}. At this moment, the capacitor is charged to the maximum level of charges $\boldsymbol{Q_{max}}$.

$$Q_{\max} = C_{\max} \cdot V_{in} \qquad [1.1]$$

The declination of the rising slope of the capacitance depends on the rise time $\boldsymbol{t_r}$ and is defined to be,

$$k_r = \frac{C_{\max}}{t_r} \qquad [2]$$

Interval 2: When the capacitance is keeping being pressed, the V_{Cvar} equals V_{in} and there is no current flowing into or out of the harvester.

Interval 3: The harvester capacitance is falling from $C_{\max}$ to $C_{\min}$. There are two subintervals of time t_{f1} and t_{f2} during the falling stage. In the time slot of t_{f1}, although the V_{Cvar} is increasing, the V_{Cvar} stays below the threshold voltage V_Z of the zener diode D_2. In this case, D_2 does not conduct yet and there is no charge transfer from C_{var} to

the load resistance R_L. Therefore, the interval of t_{f1} corresponds to a charge constrained energy conversion path. As soon as V_{Cvar} reaches V_Z, D_2 starts to conduct and the V_{Cvar} is clamped to be V_Z. That means the harvester enters the voltage constrained energy conversion stage in interval t_{f2}.

The declination of the falling slope is

$$k_f = \frac{C_{\max}}{t_f} \quad [3]$$

The time interval of t_{f1} can be calculated as following:

$$t_{f1} = \frac{C_{\max} - \frac{Q_{\max}}{V_Z}}{k_f} \quad [4]$$

The voltage over the harvester and the current through the harvester during the time interval t_{f1} and t_{f2} has been deduced as below:

$$V_{C\text{var}1} = \frac{Q_{\max} - \frac{V_{in}}{R_p} \cdot t_{press}}{C_{\max} - k_f \cdot t + t \cdot \frac{1}{R_p}} \quad [5]$$

$$V_{C\text{var}2} = \frac{\left(V_Z - \frac{V_Z}{1 - k_f \cdot R_s}\right)}{C_{mid}^{\frac{1-k_f \cdot R_s}{k_f \cdot R_s}}} \cdot (C_{mid} - k_f \cdot t)^{\frac{1-k_f \cdot R_s}{k_f \cdot R_s}} + \frac{V_Z}{1 - k_f \cdot R_s} \quad [6]$$

$$I_{C\text{var}2} = \frac{d(C_{mid} - k_f \cdot t) \cdot V_{C\text{var}}}{dt} \quad [7]$$

Interval 4: The harvester capacitor is completely released and the capacitance maintains at the minimum value $C_{\min}$. The voltage V_{Cvar} drops back to V_{in}.

The power dissipations in R_s and R_p for a complete energy harvesting cycle can therefore be written as:

$$R_{slos} = \frac{1}{T}\left(\int_0^{t_r} (V_{in} \cdot k_r)^2 \cdot R_s dt + \int_0^{t_f - t_{f1}} (-I_{C\text{var}2})^2 \cdot R_s dt\right) \quad [8]$$

$$R_{plos} = \frac{1}{T}\left(\int_0^{t_r} \frac{(V_{in} - V_{in} \cdot k_r \cdot R_s)^2}{R_p} dt + \int_0^{t_{press}} \frac{(V_{in})^2}{R_p} dt + \int_0^{t_{f1}} \frac{(V_{C\text{var}1})^2}{R_p} dt + \int_0^{t_f - t_{f1}} \frac{(V_{C\text{var}2})^2}{R_p} dt + \int_0^{t_{release}} \frac{(V_{in})^2}{R_p} dt\right) \quad [9]$$

Based on the analytical analysis above, a design example in Table 1 has been studied and the parameter analysis results regarding to the losses in R_s and R_p have been plotted in Figure 4. Figure 4(A) and (C) show the losses in percentage regarding to the ideally harvested energy. A dashed line is inserted at 20 % as an indicator how parameters have to be adapted to assure that internal losses stay below 20 %. It can be concluded that the losses in R_p are reverse proportional to the stimulating frequency of the harvester and the losses in R_p are independent of the resistance value of R_s. When the stimulating frequency is too low and the R_p is smaller than 10 GΩ, the losses in R_p are so high that the harvester could not harvest any energy at all. That means the leakage current of the harvester is decisive, whether the energy could be harvested at the desired stimulating frequency or not. The losses in R_s only happen at the rising and falling time of the capacitance variation. In the example shown $t_r = t_f = 1/(2f)$ and therefore the losses in R_s in Figure 4 have been plotted versus frequency. The losses in R_s are only slightly affected by the R_p value but strongly proportional to the frequency, namely proportional to the rising and falling times. The plots for harvested energy in Figure 4(B) and (D) show that if the losses in R_s and R_p are too high, no energy could be harvested and that's why the curves have been extended with dashed lines to below zero. Further, Figure 4(D) demonstrates that for the chosen parameters the power output is dominated by the leakage current (*Rp*) and independent for variant R_s values. This is because for higher losses in R_s the harvester could generate more energy, which is called here ideally harvested energy, but the additional generated energy is consumed inside the harvester through R_s, therefore the out coming practically harvested energy stays the same.

Table 1: Parameters used for analysis of the losses in the capacitive harvester.

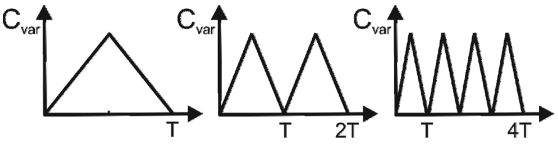

	Case 1		Case2	
Input parameters	R_s=50 kΩ	R_{p1}=1 GΩ R_{p2}=10 GΩ R_{p3}=100 GΩ	R_p=10 GΩ	R_{s1}=5 kΩ R_{s2}=50 kΩ R_{s3}=500 kΩ
	V_{in}=100 V V_z=200 V		V_{in}=100 V V_z=200 V	

It is instructive to discuss the influence of the losses on the Q-V cycle. The R_p losses result in a constant loss of charges, but as long as *D1* is conducting (Phases 1,2) those losses are compensated by additional charge flow from the input source V_{in}. Therefore, phase 3 starts with $Q_{\max}$ although the overall efficiency was reduced due to loss of charges during the charging process of the capacitor. On the other hand the R_p losses during phase 3 will actually

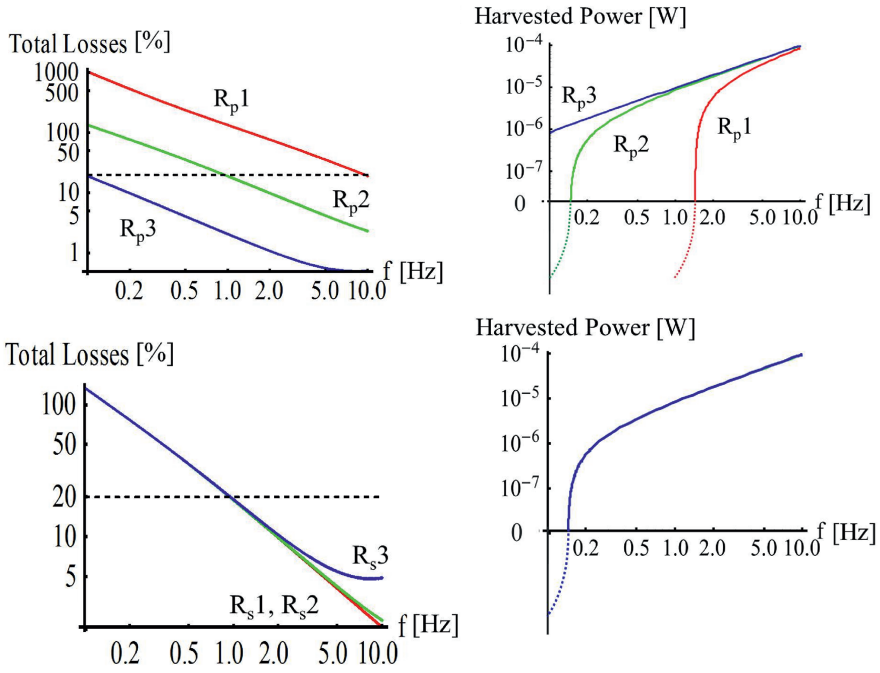

Figure 4: Numerical results of electrical losses and harvested energy for case 1; $R_s = 50$ kΩ; (A) losses in R_p and R_s in per cent of ideally harvested energy; (B) the practically harvested energy for different R_p; for case 2; $R_p = 10$ GΩ; (C) losses in R_p and R_s in per cent of ideally harvested energy, (D) the practically harvested energy for different R_s.

reduce the charges of the Q-V cycle. A charge quantity lower than Q_{max} is transferred to V_z ; the upper right corner of the QV cycle will be reduced to a value $Q_{max} - Q_{loss}$.

R_s losses are not visible in the Q-V cycle as V_{in} and V_z are constant per definition. At phase 1 the voltage over the variable capacitor is reduced by I^*R_s losses but reach V_{in} when charging is complete. During phase 3 the R_s losses are compensated by a higher voltage on the variable capacitor which is necessary to generate V_z on the output. The R_s losses in phase 3 would only be critical if R_p is relevant as leakage increases with rising voltage or if the break down voltage of the variable capacitor is reached. During phase1 high R_s values may lead to a high time constant and insufficient charging in case of short rise time t_r.

Experimental

Sample Preparation and Measurement Set-up

The elastomer-electrode was prepared with help of an electrically conductive silicone rubber "ELASTOSIL® LR 3162 A/B" (Wacker Chemie AG), a two-component compound with short curing time. The electrical conductivity is 11 Ωcm and the viscosity is 6,600 Pas according to the data sheet. Doctor blade as well as screen printing was used to deposit the material on copper foil or flexible printed circuit board material. Curing was done for 3 h at 70 °C.

Three types of dielectric were tested: sputtered Al_2O_3 and Ta_2O_5 on silicon substrate, PET films and screen printed composite dielectrics.

1.4 µm thick dielectric BoPET foils (Biaxially-oriented polythelene terephthalate, DuPont Teijin Films, trade name "Mylar", PET) were laminated onto metal substrates. The dielectric constant and break down voltage is 3.25 and 280 V/µm respectively.

The fabrication process is split into two stages: deposition and fusing with the substrate. Under particle free atmosphere in a flow box the PET-foil is unrolled onto the substrate, cut into optimal dimensions and smoothed with a felt blade to eliminate wrinkles. To melt the foil onto the substrate, it is heated on a hotplate at 260 °C for 10 s.

The screen printing of composite dielectric was done at EURECAT (www.matflexend.eu]) with a novel material developed at IMPERIAL College London (Leese et al. 2016). Strontium doped barium titanate (SBTO) nano fibers were functionalized to improve the wetting between the filler and matrix (epoxy or PVDF).

Dielectric and elastomer electrode foils were mounted in a mechanical cycling station that allowed to adjust the maximum force and cycle frequency. All measured samples had a size of 10 × 10 mm^2.

The capacity as function of the applied force was measured with help of Agilent 4284A RLC meter. The leakage current was measured at 100 V with Keithley 2450 source meter. A steady state value was achieved after ca. 3 min. For current/charge measurements according to Figure 3(A) the source meter was used as input voltage source (V_{in} = 100 V) and for measurement of the input current. The output current was measured over R_L with help of the oscilloscope 3012(B). In a second configuration the Zener diode D_2 was replaced with a diode identical to D_1 and R_L was replaced by a 3.3 nF capacitor. The transferred charges were calculated based on the increase of the voltage at the output capacitor

Measurements

For initial characterization of the dielectrics metal contacts were sputtered on top of the dielectrics. The obtained capacity per area was in good agreement with the values calculated from thickness and dielectric constant (Table 2). The leakage current at 100 V was in all cases below 1 nA which corresponds to an R_p value of 100 GΩ according to Section "Calculation of Losses with the Equivalent Circuit Model". Some of the sputtered and screen printed dielectric layers showed higher leakage currents due to defects and were excluded from the experiments. The electrical resistance of the elastomer electrode was measured by pressing it against a metal foil. Values between 3 and 5 kΩcm^2 at 30 N/cm^2 were obtained which saturated at a pressure higher than 80 N/cm^2 at values between 1 and 3 kΩcm^2. Thus both, R_s and R_p were in the required range for efficient energy harvesting according to the calculations in Section "Calculation of Losses with the Equivalent Circuit Model".

Table 2: Parameter of investigated dielectrics. Theoretical and measured capacity, measured leakage current at 100 V.

Dielectric	Thickness	k	C′	C′ measurement	Leakage current
	µm		nF/cm^2	nF/cm^2	nA/cm^2
Ta_2O_5	1.0	26	23	22.4	0.26 … 0.4
Al_2O_3	0.5	9	16	14.6	0.90 … 1.1
PET	1.4	3.3	2.1	–	<1
SBTO	35	36	0.91	0.85	<1 selected

Figure 5 shows the specific capacity (capacity per area) as function of mechanical pressure that was achieved with the elastomer top electrode in contact with all investigated dielectric samples. As demonstrated in Figure 5(C) the values are much lower than the corresponding capacitance with thin film metal electrode. The similarity to the behavior shown in Figure 2(C) is obvious – the higher the theoretical capacity the larger the discrepancy with the capacity obtained with elastomer electrode. Although the bulk conductivity of the elastomer is quite low, the mean distance of the electrical conducting phase at the interface may be too large. Surface roughness of both, dielectric and elastomer electrode plays also an important role. The mean roughness of thin film and PET dielectric was below 1 nm while the thick film dielectric showed a roughness of ca. 30 nm. This results in lower capacity in the low force region on the rough surface as can be seen in Figure 5(B). In another experiment elastomer electrodes were fabricated with a rough surface to reduce the sticking behavior between electrode and dielectric, but these samples showed further reduced maximum capacity (Figure 5(C), open symbols).

Precise current measurement turned out to be critical due to the limited time resolution of the equipment and the short current pulses especially during discharge of the variable capacitor. Thus, we did not use the measuring circuit according to Figure 3(A) but have replaced the Zener diode by a diode similar to *D1* and measured the voltage increase at the 3.3 nF output capacitor which replaced R_L shown in Figure 3(A).

Figure 6(A) and (B) show the influence of pressing force and cycle time on the harvesting performance of elastomer electrode on PET dielectric. The observed faster voltage increase at shorter cycle time is a result of leakage currents (Figure 6(B)).

As the specific capacity is limited due to the used elastomer electrode, the foil technology was used to fabricate a stack three capacitor layers (Figure 7) to increase the power density. The voltage rise shown in Figure 6(C) was achieved with the resulting maximum capacity of ca. 1.5 nF. Printed SBTO dielectric was used for the stacked devices.

The novel printed composite dielectric results in nearly the same capacitance as the PET foil bus show much better mechanical robustness due to the higher thickness. This is important for a device were the electrode will be pressed thousands to million times against the dielectric. On the other hand point defects were observed in several samples of the printed dielectrics which lead to leakage current and the deposition process must still be improved.

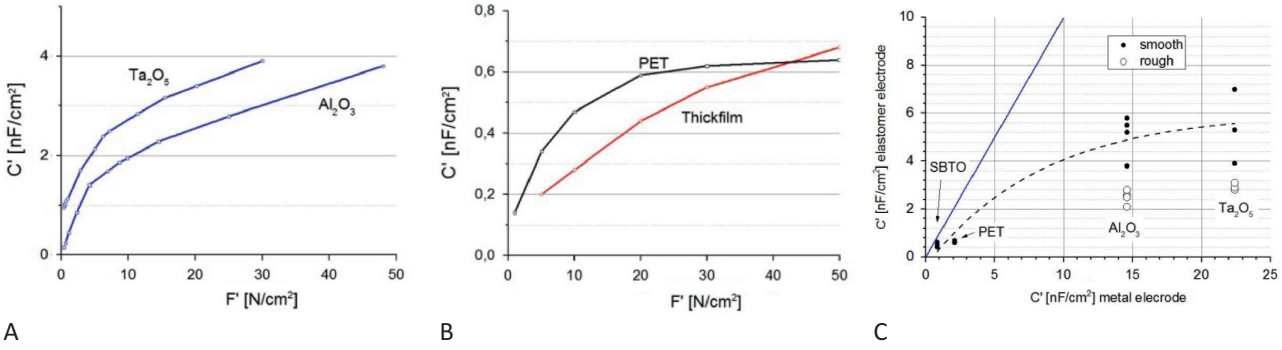

Figure 5: Specific capacity of tested dielectrics in contact with elastomer electrode as function of mechanical pressure; (A): thin film dielectric, (B): thick film and polymer foil dielectric, (C) specific capacity obtained with elastomer electrode at 50 N/cm^2 as function of the regular capacity with metal electrode.

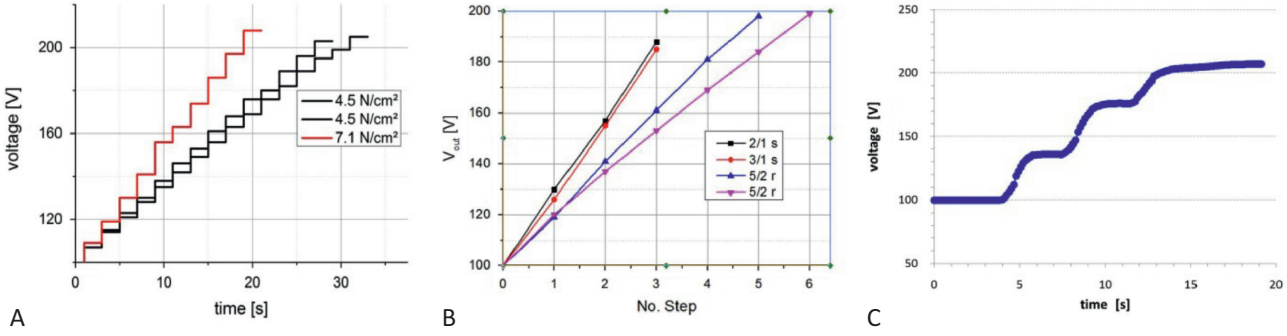

Figure 6: Voltage rise at output capacitor during cycling of the variable capacitor; (A) variation of maximum pressing force (C_{max} = 240 pF, 370 pF for 4.5 and 7.1 N/cm^2 respectively), (B) variation of cycle time (2 ... 5 s in pressed state, 1 ... 2 s release, C_{max} = 770 pF), (C) voltage rise of three layer stacked variable capacitor according to Figure 7.

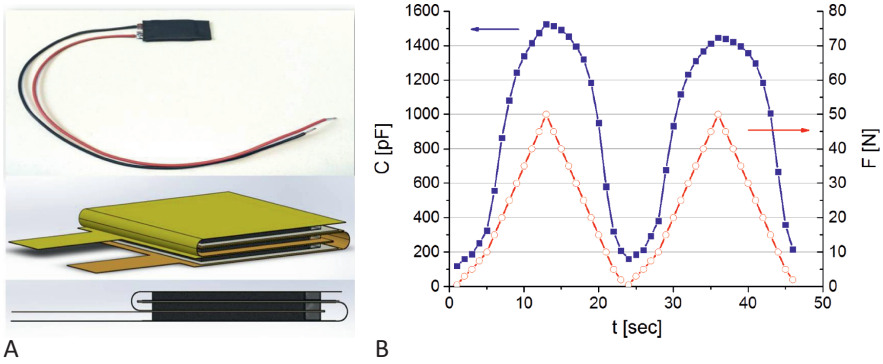

Figure 7: Three layer stack harvester demonstrator, A = 1 cm^2, (C_{max} = 1.5 nF, C_{min} = 180 pF); (A) design sketch and packaged device, (B) capacity as function of applied force.

The demonstrator was fabricated based on flexible printed circuit technology and screen printing that will allow later low cost fabricate on. The design (Figure 7(A)) and process for a folded multi-layer harvester including the encapsulation was developed and several samples of harvester devices have been tested. Spacer structures between electrode and dielectric have been introduced to allow quick detachment and low C_{min} values after pressure release.

Figure 7(B) shows how capacity is changing as function of the applied mechanical force on the tree layer capacitor stack. The remaining capacity at zero force is ca. 200 pF,

hence the maximum capacity is ca. 7.5 times higher than the minimum capacity; much more than values achieved with typical variable MEMS capacitors. This results in a large Q-V rectangle of the harvesting cycle (Figure 3(B)). At forces higher than 40 N the capacity increase becomes smaller and reaches saturation at ca. 50 N as can be seen from the rounded shape of the capacity curve.

Conclusions

The capacitive energy harvesting principle with elastomer electrode was proven. Numerical simulation was used to identify the influence of material parameters and parasitic circuit elements on the harvester performance as function of actuation frequency. The equivalent circuit model indicated that losses in the serial resistance R_s are only a function of rise and falling times of the capacitor changes. R_s values are not critical as long as they are below 10 kΩ. For typical low frequency operation (0.1 ... 10 Hz) R_p should be above 10 GΩ per square centimeter.

FEM simulations and experimental results clearly indicate that the specific capacity is not limited by the dielectric material but due to the elastomer electrode. No more than ca. 1 nF/cm^2 can be practically achieved with the used commercial conducting elastomer. Further materials research is required to synthetize low viscosity conducting elastomers with high surface conductivity.

A capacity of 650 pF/cm² was achieved with novel screen printed dielectrics and commercial elastomer electrodes. Charges between 25 and 70 nAs per cm^2 have been transferred per cycle at 100 V/200 V. At an actuation frequency of ca. 1 Hz this corresponds to 0.5 ... 1.5 μW/cm^2.

A foil stack technology was developed based on folding of printed dielectric and elastomer layers on metal foils.

Future work will focus on increasing the power density based on new elastomer electrodes, increasing the screen print yield and investigation the long term cycle stability. Harvester variants will be optimized for low and higher force applications. Another aspect concerns the adaption of an electronic circuit interface which will allow the charge of a battery with the capacitive harvester.

Acknowledgements: This work is part of the MATFLEXEND project funded by the European Union under contract 604093 (www.matflexend.eu). Special thanks go to the Milo Shaffer group at Imperial College London for synthesis of composite dielectrics and to EURECAT for printing trials.

References

Galayko, D., and A. Dudka. 2015. "Capacitive Energy Conversion with Circuits Implementing a Rectangular Charge-Voltage Cycle—Part 1: Analysis of the Electrical Domain." *IEEE Transactions on Circuits* 62:11. doi:10.1109/TCSI.2015.2451911.

Hsu, T., S. Manakasettharn, J. A. Taylor, and T. Krupenkina. 2015. "Bubbler: A Novel Ultra-High Power Density Energy Harvesting Method Based on Reverse Electrowetting." *Scientific Reports* 5: 165372011, 2:448.

Janssen, M., B. Werkhoven, and R. van Roij. 2016. "Harvesting Vibrational Energy with Liquid-Bridged Electrodes: Thermodynamics in Mechanically and Electrically Driven RC-Circuits." arXiv:1603.04315v1 [physics.comp-ph].

Krupenkin, T., and J. A. Taylor. 2011. "Reverse Electrowetting as a New Approach to High-Power Energy Harvesting." *Nature Communications* 23:448.

Leese, H., J. Morávková, H. C. Yau, M. Tejkl, J. Buk, and M. Shaffer. 2016. "Polymer Functionalised Strontium Doped Barium Titanate Nanofiber Composites for High-k Dielectrics." E-MRS spring meeting, Lille 2016, 2–6 May 2016.

Lu, Y., F. Cottone, and S. Boisseau. 2016. "Low-Frequency and Ultra-Wideband MEMS Electrostatic Vibration Energy Harvester." IEEE, 10.1109/MEMSYS.2016.7421550

Lv, X., L. Liu, Y. Liu, and J. Leng. 2015. "Dielectric Elastomer Energy Harvesting: Maximal Converted Energy, Viscoelastic Dissipation and a Wave Power Generator." *Smart Materials and Structures* 24:11.

Sheu, G.-J., et al. 2011. "Development of a Low Frequency Electrostatic Energy Harvester." *Sensors and Actuators* A167:70.

Zhang, J., Y. Wang, H. Chen, and B. Li. 2015. "Energy Harvesting Performance of Viscoelastic Polyacrylic Dielectric Elastomers." *International Journal of Smart and Nano Materials*. DOI: 10.1080/19475411.2015.1092480.

www.matflexend.eu.

Note: This paper contains original research which was not published elsewhere before. A presentation was given at the E-MRS 2016 in Lille, Symposium W.